RESEARCH ARTICLE | DECEMBER 29 2022

Effectiveness of plexiglass barriers in mitigating spread of aerosolized droplets in a cough

Manhar Dhanak; Adriana McKinney; Siddhartha Verma; ... et. al

Physics of Fluids 34, 125137 (2022)
https://doi.org/10.1063/5.0129635

Physics of Fluids ARTICLE scitation.org/journal/phf

Effectiveness of plexiglass barriers in mitigating spread of aerosolized droplets in a cough

Cite as: Phys. Fluids **34**, 125137 (2022); doi: 10.1063/5.0129635
Submitted: 6 October 2022 · Accepted: 30 November 2022 ·
Published Online: 29 December 2022

Manhar Dhanak,[a] Adriana McKinney,[b] Siddhartha Verma,[c] and John Frankenfield[d]

AFFILIATIONS

Department of Ocean and Mechanical Engineering, Florida Atlantic University, Boca Raton, Florida 33431, USA

Note: This paper is part of the special topic, Flow and the Virus.
[a]**Author to whom correspondence should be addressed**: dhanak@fau.edu
[b]Electronic mail: amckinney2016@fau.edu
[c]Electronic mail: vermas@fau.edu
[d]Electronic mail: jfranken@fau.edu

ABSTRACT

Plexiglass barriers have been prevalently used in the workplace during the Covid-19 pandemic as protective measures against the airborne transmission of severe acute respiratory syndrome coronavirus 2 (SARS-CoV-2) through interactions between potentially infected and uninfected individuals. Doubts have been raised about their effectiveness and concerns have even been expressed about the implications for room ventilation on their overuse. To aid public awareness of the role of such plexiglass barriers, we use flow visualization, aided by particle count measurements, to examine in a laboratory setting the effectiveness of typical workplace barriers in impeding the spread of aerosol-size airborne droplets. Such droplets are emitted in coughs and other respiratory exhalations and serve as modes of transmission for viruses. The visualizations and the supporting particle count measurements indicate that barriers do impede the forward momentum of the droplet-laden airflow jet that result from a cough, but portions of the expelled aerosols can spread around the barriers. Our study suggests that in comparison with the case in the absence of a barrier, a 2.5 ft or higher barrier can reduce the concentration levels of aerosols of size $<10\,\mu$m on the side of the barrier away from the source by over 90% and those of size $<3\,\mu$m by over 82%. However, an opening at the bottom of a barrier, for example, representing access for transactions between a worker and customers, can significantly reduce the effectiveness of the barrier. Finally, we illustrate how the aerosol dispersion in this case can be dramatically altered by ambient background airflows.

I. INTRODUCTION

Respiratory exhalations, during breathing, talking, coughing, and sneezing, contain droplets of sizes that range from over 50 μm to less than 10 μm (aerosols) and serve as modes of transmission for pathogens that may be smaller than 1 μm, as in the case of the severe acute respiratory syndrome coronavirus 2 (SARS-CoV-2) responsible for the Covid-19 pandemic.[1] The larger droplets fall to the ground within a short distance of the source due to gravity, but the aerosolized droplets, being resisted by air friction, fall very slowly.[2,3] They can, therefore, remain suspended in air for several minutes and travel much farther from the source due to the forward momentum of the expiratory jets, coupled with prevailing air flow in the room.[4]

During the pandemic, the centers for disease control (CDC) recommended minimum social distancing of 6 ft to mitigate risk of exposure. Indoor workplace settings, where the recommended social distancing may not be feasible, can serve to promote transmission of airborne infections.[5] In such settings, use of plexiglass barriers became commonplace during the Covid-19 pandemic in many workplace settings, including checkout counters at groceries, nail salons, and open-plan offices involving workers interacting with customers or other workers in proximity, as well as in settings where healthcare workers may be exposed to the infection. Barriers were also implemented on student desks in classroom settings involving students interacting among themselves and with teachers. The aim of a barrier is to impede the passage of droplets present in respiratory exhalations of an infected person on one side of the barrier to the other side. However, experimental studies[6–8] as well as computational studies[9–14] in various settings show mixed results. Epidemiologists point out that barriers do not eliminate the aerosolized droplets from spreading around them and may result in giving people false sense of protection from exposure to viral infections (see, for example, Ref. 15). Furthermore, they note that presence of multiple barriers in a room likely impedes the overall ventilation in the room, which over time may result in the accumulation of the potentially infected aerosol-size

droplets in the room and increase the risk of viral transmission. Others suggest that the use of barriers in certain settings, may still be appropriate, provided they are properly engineered, including consideration of the type and size of barriers and their impact on the ventilation in the room. A recent cough-simulator based laboratory investigation by Bartels *et al.*[16] examined the roles of height and width of plexiglass barriers with a small opening at the bottom, representing access for transactions, in mitigating the spread of expiratory droplets from a cough. Particle count measurements were made on either side of each barrier following a simulated cough that resulted in emission of aerosol-size droplets. Barriers at least 3 ft high and 3 ft wide were shown to be effective in reducing the count of aerosols (sized $< 3\ \mu$m) on the side of the barrier away from the cough simulator by around 70% and those of size 3.5–6.25 μm by over 61%–69%.

In response to these studies, government agency guidelines on use of plexiglass barriers have undergone change. Currently, the CDC recommends use of barriers as added benefit to social distancing and masking, particularly at reception and triage locations and specific pathways in healthcare settings.[17] The National Institutes of Health suggests barriers in the workplace may provide added droplet protection in locations with frequent, short duration contact with external personnel.[18] The Environmental Modeling Group of the UK Government[19] suggests the need for further study, particularly using flow visualization.

The primary objective of the present laboratory study is to provide flow visualization, supported by particle count measurements, of the spread of aerosolized droplets emitted from respiratory exhalations in the presence of barriers. In our previous related work,[20] we found that in still air, in the absence of a barrier, aerosolized droplets emitted in a simulated cough could travel over 6 ft from the source and remain suspended in the air for several minutes. Here, we describe an extension of that study to consider the impact of plexiglass barriers of the kind implemented in typical workplace settings on the spread of aerosolized droplets ($\leq 10\ \mu$m) from simulated coughs. In contrast to Ref. 16, we examine the impact of the presence of an opening (representing an opening for transactions) at the bottom of an adequately sized barrier on the effectiveness of the barrier and illustrate how ambient airflows can impact the results. We provide visualization of the dispersion of the aerosols, supported by particle count measurements at multiple locations. Estimates of the relative mass concentration levels of the aerosols on the cough simulator side of the barrier and at locations on the other side of the barrier both close to and away from the barrier are provided.

II. METHODOLOGY

A cough is simulated mechanically via a cough simulator consisting of a mannequin with a hollow head that is connected to a source generating tracers composed of heated droplets of distilled water and glycerin, previously described in Refs. 20 and 21. Air, when released from a pressure-regulated reservoir connected to the mannequin, impulsively pumps 1.9 l of air mixed with the water droplets out through the mannequin's mouth; the reservoir is in the form of a fixed-volume container to which pressurized air is supplied via a ball valve utilizing a pressure regulator to maintain air at a selected pressure level in the container before it is discharged via a trigger valve to simulate a cough. Most of the aerosol-size droplet tracers generated are of size $\leq 6\ \mu$m. The volume of air is comparable to that of a mid-level adult cough and this range of droplet size correspond to the lower end of aerosol-size droplets emitted in a cough and span the inhalable ($\leq 10\ \mu$m) and respirable ($\leq 5\ \mu$m) ranges of particles. An estimated 97 μl of tracer fluid is emitted in the cough [Eq. (1)].

The schematic and a complementary photograph of the laboratory setup are provided in Fig. 1. The mannequin simulating the cough was placed 20 in from the barrier, representing an individual seated behind a barrier; the mannequin was vertically and horizontally centered behind the barrier so that the top of the barrier was 15–18 in above the mannequin's mouth. The mannequin side of the barrier is designated here as the inside, and the other side of the barrier as the outside. The tracer droplets emitted in a cough were visualized as they spread, using multiple laser sheets to capture the spatial and temporal development of the ensuing flow. Laser light source A enabled observation of the spreading droplets in both a vertical laser sheet aligned with the sagittal plane as well as in a horizontal light sheet aligned with the position of the mouth of the mannequin. Laser light source B enabled observation of the spread of the droplets in a cross plane in the boundary layer along the inside surface of the barrier. The three laser sheets provide visualization of the volumetric spread of the droplets in the exhaled airflow. The camera was located on the side opposite the laser light sources for best visualization, considering that the droplets scatter light preferentially in the direction away from the light source.

The visual observations were complemented by particle count measurements using optical particle counters (OPC-N3) from Alphasense Ltd. The OPC-N3 sensor has been evaluated against a benchmark Grimm aerosol spectrometer by Sousan *et al.*[22] In cases of

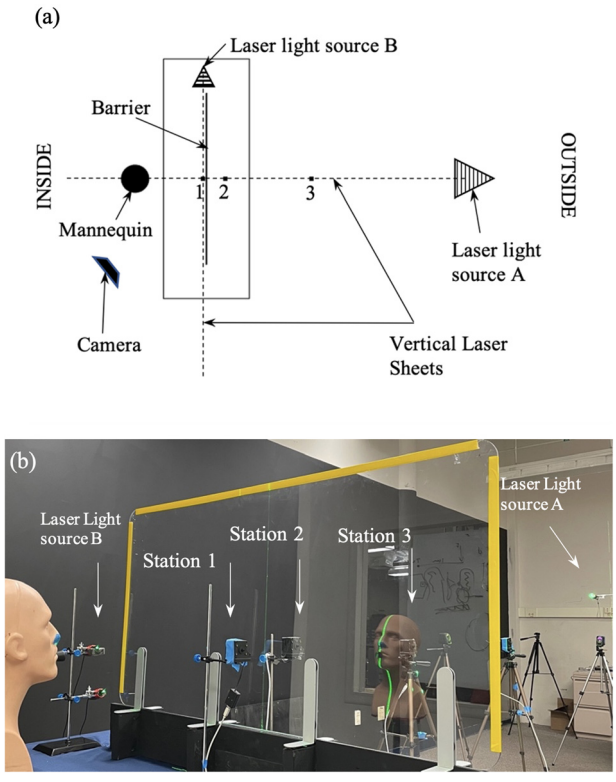

FIG. 1. (a) Schematic (top view) and a photograph (b) of the laboratory setup, showing positions of OPC stations 1, 2, and 3 relative to the barrier.

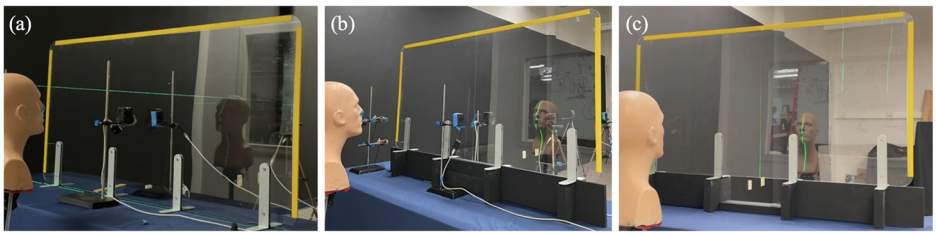

FIG. 2. (a) 2.5, (b) 3, and (c) 3 ft barriers with a 5×12 in opening underneath. Each barrier is approximately 5 ft wide.

mid to high level aerosol concentration settings, such as the case of the present laboratory study, the authors showed that various types of aerosols measurement of $PM_{2.5}$ and PM_{10} with a OPC-N3 sensor were highly linear with the reference spectrometer, with corresponding correlation coefficient ($r > 0.97$), slope, and intercept values meeting Environmental Protection Agency (EPA) and National Institute of Occupational Safety and Health (NIOSH) criteria.

Three OPC-N3s were placed at the same height as the mannequin's mouth on tripods located at three observation stations ahead of the mannequin as indicated in Fig. 1. Station 1 was located on the inside, 2.5 in from the barrier and stations 2 and 3 were located on the outside, respectively, 6 in and 3 ft from the barrier; Stations 2 and 3 were approximately 2.2 and 4.75 ft, respectively, from the mannequin. An additional particle counter placed 7.7 ft downstream of the mannequin did not register readings measurably different from the ambient and the associated observations are, therefore, not included here.

Three types of plane plexiglass barriers were considered: a 2.5 ft high barrier, a 3 ft high barrier, and a 3 ft high barrier with a 5×12 in gap or opening underneath [Figs. 2(a)–2(c)]. Such barriers may be found in various workplace settings. The opening beneath a barrier may represent an opening to facilitate access for transactions between a worker and a customer, such as in a nail salon or a checkout counter at a grocery store. Three sets of the following four tests were conducted in a laboratory setting involving: (1) absence of any barrier (as a control experiment), (2) the 2.5 ft high barrier, (3) the 3 ft high barrier, and (4) the 3 ft high barrier with the opening at the bottom of the barrier. The temperature and relative humidity in the laboratory were, respectively, 22 °C and 47%, typical of an air-conditioned indoor environment. The air-conditioning inflow in the vicinity of the apparatus was controlled to minimize any ambient airflow while these tests were conducted.

III. RESULTS

The measurements were made simultaneously and synchronized using a single computer for data acquisition from the three sensors. Each OPC records particle counts in 24 bins of mean diameter sizes ranging from 0.4 to 40 μm over 1 s time intervals using a mean sampling flow rate. The contribution of aerosols in the PM_N range (particles of size $d_i < N\,\mu$m) to the mass concentration $\sigma_{jk}^{PM_N}(t)$ of the tracer fluid at an observation station j ($j = 1, 2, 3$) for case k ($k = 1, 2, 3$, and 4, respectively, for the cases with (1) no barrier, (2) 2.5, (3) 3, and (4) 3 ft barriers with an opening) is estimated as

$$\sigma_{jk}^{PM_N}(t) = \sum_{i \in PM_N} \frac{\rho \pi n_{ijk} d_{ijk}^3}{6 Q_{sjk}} \left(\frac{\mu g}{m^3}\right), \tag{1}$$

where n_{ijk} is the count per second of particles of mean diameter d_{ijk}, Q_{sjk} is the sampling flow rate, and $\rho = 1.065\,g/cm^3$ is the density of the tracer fluid; $Q_{sjk} \simeq 2.6\text{–}4.9 \times 10^{-6}\,m^3/s$. Particle counts of size $>10\,\mu$m were insignificant at all observation stations. We, therefore, consider here the dispersion distributions of PM_{10} (particles of size $d_{ijk} < 10\,\mu$m) and PM_3 (particles of size $d_{ijk} < 3\,\mu$m). The rolling mean mass concentrations $\overline{\sigma_{jk}^{PM_3}}(t)$ and $\overline{\sigma_{jk}^{PM_{10}}}(t)$ at each of the stations ($j = 1, 2, 3$) for the four test cases ($k = 1, 2, 3, 4$) are also computed over the observed time $t = t_e$ and the mean concentrations over the period of observation, $\overline{\sigma_{jk}^{PM_3}}(t_e)$ and $\overline{\sigma_{jk}^{PM_{10}}}(t_e)$, are provided in Table I; these computations are consistent with the concentrations computed by algorithms embedded in the sensors, provided the sensor concentration data are corrected for the actual density of the tracer fluid $\rho = 1.065\,g/cm^3$ instead of $1.65\,g/cm^3$ set in the sensor algorithm.

A. No barrier case ($k = 1$)

The spread of the aerosols from the simulated cough in the absence of the barrier is depicted in a sequence of captured images in Figs. 3(a)–3(c) (Multimedia views). The spread is in the form of an impulsively started turbulent jet expanding in a 24° cone as it entrains

TABLE I. Mean concentration $\overline{\sigma_{jk}^{PM_{10}}}(t_e)$ and, $\overline{\sigma_{jk}^{PM_3}}(t_e)$ ± one standard deviation of the rolling mean over the observation period $t = t_e$ at each of the three stations ($j = 1, 2, 3$,) for the cases of no barrier, 2.5, 3, and 3 ft barriers with an opening ($k = 1, 2, 3, 4$).

	PM_{10} concentration (mg/m^3)			PM_3 concentration (mg/m^3)		
	Station 1	Station 2	Station 3	Station 1	Station 2	Station 3
No barrier ($k = 1$)	0.115 ± 0.057	0.094 ± 0.043	0.01 ± 0.005	0.073 ± 0.054	0.066 ± 0.041	0.009 ± 0.005
2.5 ft barrier ($k = 2$)	0.194 ± 0.072	0.021 ± 0.009	0.003 ± 0.004	0.099 ± 0.056	0.014 ± 0.004	0.002 ± 0.001
3 ft barrier ($k = 3$)	0.153 ± 0.070	0.014 ± 0.017	0.009 ± 0.013	0.086 ± 0.064	0.005 ± 0.002	0.003 ± 0.001
Barrier with an opening ($k = 4$)	0.178 ± 0.063	0.075 ± 0.035	0.016 ± 0.013	0.127 ± 0.057	0.059 ± 0.026	0.009 ± 0.007

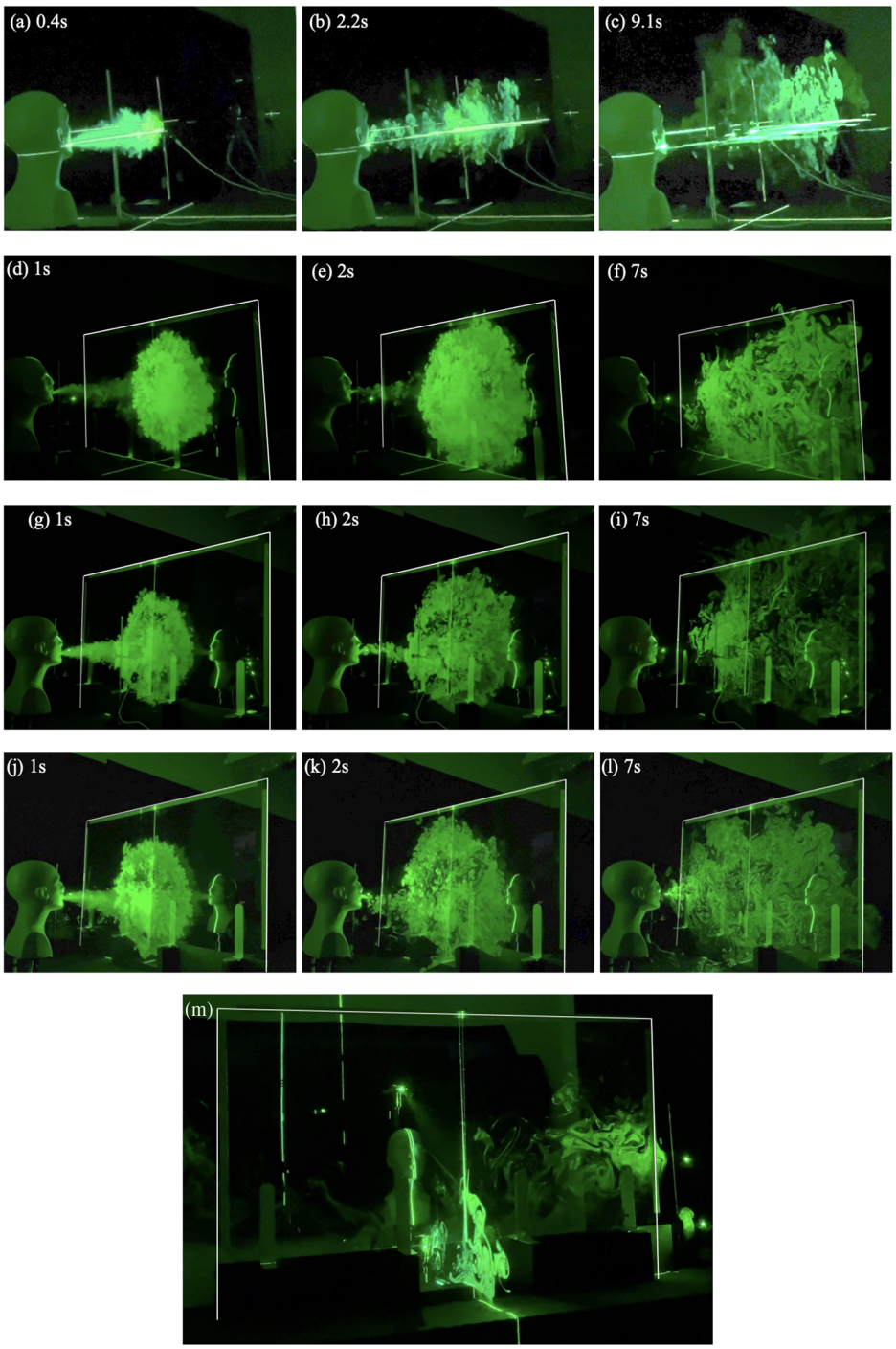

FIG. 3. Comparison of the dispersion of aerosolized droplets from a simulated cough in cases with and without a barrier: Dispersion of aerosols in the absence of a barrier (a)–(c), dispersion of aerosols in the presence of a 2.5 ft barrier without an opening (d)–(f), a 3 ft barrier without an opening (g)–(i), and a 3 ft barrier with an opening at the bottom (j)–(l). The times elapsed following a cough are shown in the insets. The edges of the barrier are outlined in white. Figure 3 (m) depicts the case of the 3 ft barrier with an opening at the bottom as viewed from outside of the barrier at 13 s following a simulated cough. Multimedia views: https://doi.org/10.1063/5.0129635.1; https://doi.org/10.1063/5.0129635.2; https://doi.org/10.1063/5.0129635.3; https://doi.org/10.1063/5.0129635.4; https://doi.org/10.1063/5.0129635.5

the surrounding air, with a leading puff or vortex ring that expands correspondingly. An analysis of video imagery, corresponding to Figs. 3(a) and 3(b), suggests that an initial distance traveled by the leading edge of the jet is proportional to $t^{1/2}$, typical of an impulsively generated jet. The velocity at the mouth of the mannequin (a nozzle with a diameter of 1.3 cm) is estimated to be approximately 50 cm/s. Further downstream, the forward motion is slower; theoretical considerations based on conservation of mass and momentum and self-similar flow profiles suggest that the centerline speed of the jet decays as $\sim 1/x$, where x is the axial distance from the source, and the flow across a

cross section follow a Gaussian distribution.[23] As a result, the droplets spread three-dimensionally, as can be seen from the visualization in the horizontal laser sheet in Fig. 3(c).

Particle count measurements of the aerosol-size droplets at the three observation stations over the period of the spread are shown in Figs. 4(a)–4(c) for particles in the PM_{10} range, that is, particles of size $<10\,\mu$m. Particle count measurements at stations 1 and 2 [Figs. 4(a) and 4(b)] in the absence of a barrier are almost identical, since these observation stations are close to each other, respectively, representing observations on either side of the position of the barrier, but with the barrier absent in this case. Significantly reduced particle counts are recorded at station 3 [Fig. 4(c)], approximately 4.75 ft downstream of the mannequin. The distribution of the total particle counts across particle size over the period of observation at each of the three stations in the absence of a barrier is shown in Fig. 5(a). The particle sizes are dominantly $<4\,\mu$m, corresponding to the respirable range. The distributions at stations 1 and 2 are similar and feature a characteristic peak at $d_i = 1.5\,\mu$m mean droplet diameter. The time series of the mass concentrations for the case of no barrier, $\sigma_{j1}^{PM_{10}}(t)$, at the three stations $(j = 1, 2, 3)$ are shown in Fig. 6(a) and the corresponding rolling mean contributions $\overline{\sigma_{j1}^{PM_{10}}}(t)$ and $\overline{\sigma_{j1}^{PM_3}}(t)$ of PM_{10} and PM_3 aerosols are shown in Fig. 6(e). As expected, the mass concentration $\sigma_{21}^{PM_{10}}(t)$ at station 2 closely matches the concentration $\sigma_{11}^{PM_{10}}(t)$ at station 1, in view of the proximity of the two stations. The rolling mean mass concentrations, $\overline{\sigma_{j1}^{PM_N}}(t)$ $(j = 1, 2, 3; N = 3, 10)$, are shown in Fig. 6(e). At station 2, the mean concentrations $\overline{\sigma_{21}^{PM_{10}}}(t_e)$ and $\overline{\sigma_{21}^{PM_3}}(t_e)$ over the period of observation $(t = t_e)$ are, respectively, 82% and 90% of the corresponding concentrations $\overline{\sigma_{11}^{PM_{10}}}(t_e)$ and $\overline{\sigma_{11}^{PM_3}}(t_e)$ at station 1

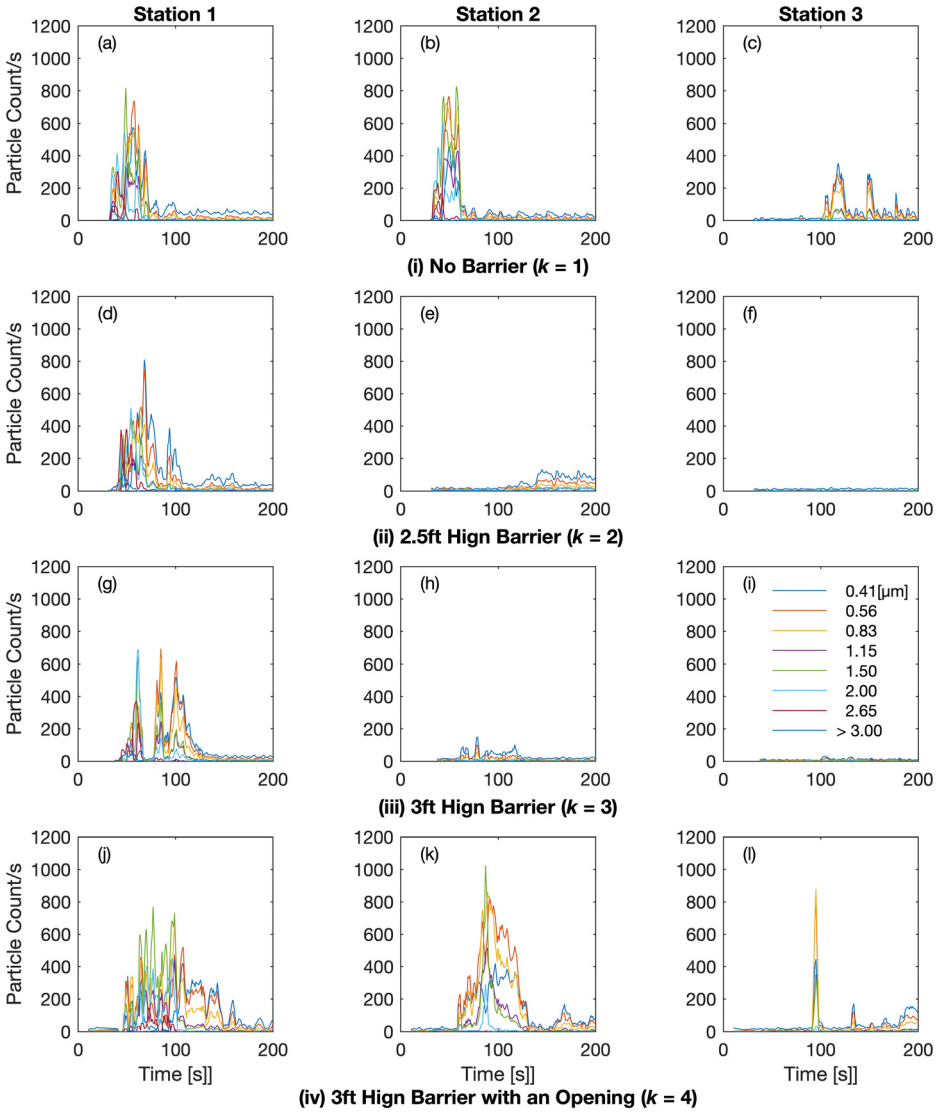

FIG. 4. (a)–(l) Particle count measurement of the aerosolized droplets at each of the three observation stations over the period of observation.

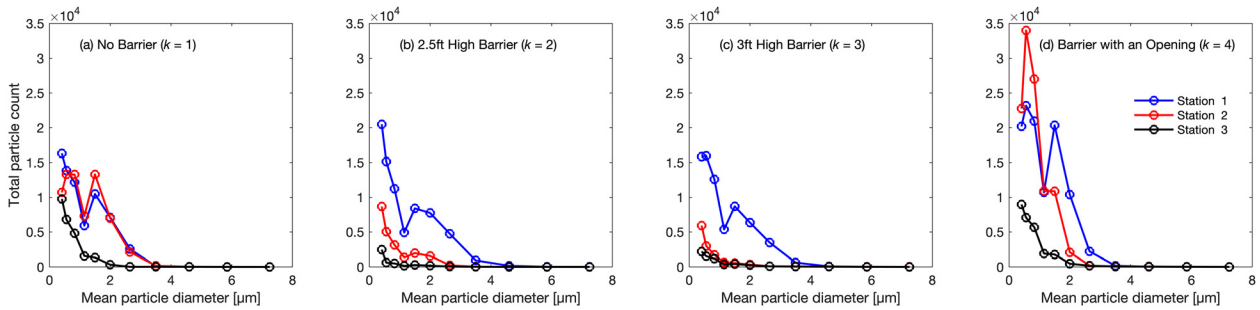

FIG. 5. (a)–(d) Comparison of the distribution of total particle count over the observation period as a function of the particle size.

(Table I). At station 3, the mean concentrations $\overline{\sigma_{31}^{PM_{10}}}(t_e)$ and $\overline{\sigma_{31}^{PM_3}}(t_e)$ are, respectively, 9% and 12% of the corresponding concentrations $\overline{\sigma_{11}^{PM_{10}}}(t_e)$ and $\overline{\sigma_{11}^{PM_3}}(t_e)$ at station 1.

B. Cases of 2.5 and 3 ft barriers without any openings ($k = 2, 3$)

Figures 3(d)–3(f) and 3(g)–3(i), respectively, depict the sequence of captured images of the spread of the simulated cough in the presence of the 2.5 and 3 ft high barriers with no openings in the barrier. The images show how the turbulent jet spreads in an expanding vortex ring [Figs. 3(d), 3(e), 3(g), and 3(h)] in the boundary layer on the surface of the barrier once the jet impinges onto the barrier and is deflected away from the axis of the cough jet. The boundary layer away from the stagnation region of the impingement thickens as it spreads as a wall jet across the barrier.[23]

A portion of the aerosol-size droplets spreads over and around the barrier [Figs. 3(f) and 3(i)]. However, with the loss of the forward momentum, most of the droplets appear to be contained on the inside of the barrier, at least in the short term.

The particle count measurements at the three stations ($j = 1$, 2, 3) for these two cases are, respectively, shown in Figs. 4(d)–4(f) and 4(g)–4(i). In contrast to the case in the absence of the barrier, the elevations in the particle count measurements at station 2 [Figs. 4(e) and 4(h)] immediately on the outside of the barrier are much smaller than the corresponding levels at station 1 on the inside of the barrier [Figs. 4(d) and 4(g)] or at station 2 [Fig. 4(b)] in the absence of the barrier, consistent with the visual observations. Elevations in particle counts, above the ambient levels, were apparent at station 3 [Fig. 4(f) and 4(i)]. The distributions of the total particle count over the period of observation in the case of the 2.5 and 3 ft barriers without any openings are shown in Figs. 5(b) and 5(c), respectively. The total particle counts across the range of particle sizes at station 1 on the inside of the barrier are similar to those in the absence of the barrier. However, they are significantly smaller in magnitude at stations 2 and 3 on the outside of the barrier. These observations are reflected in comparing the mass

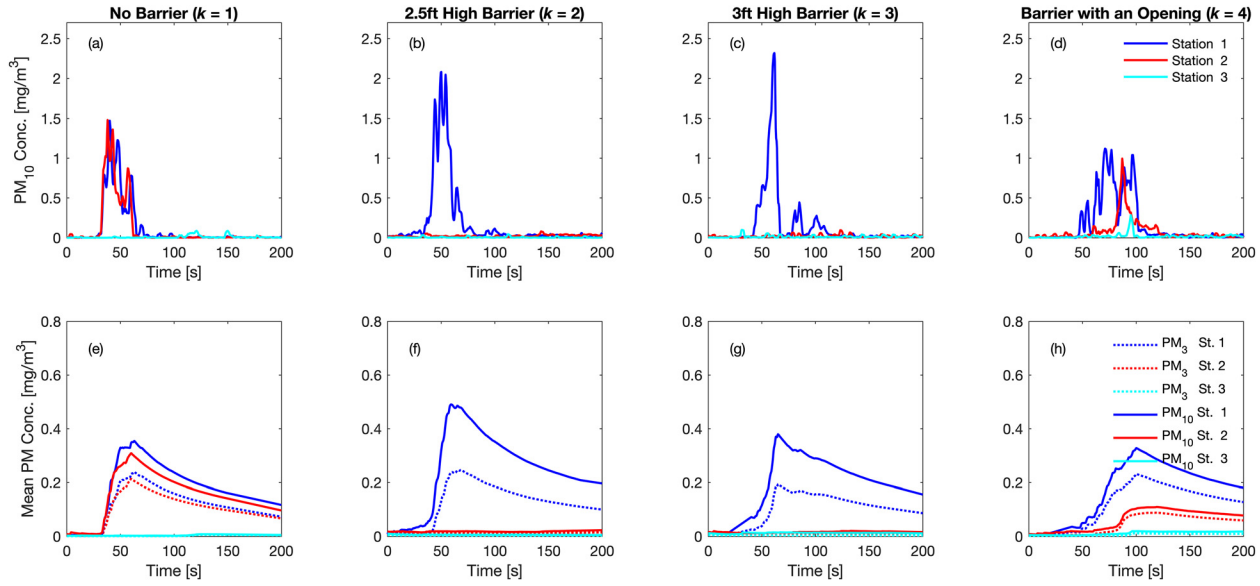

FIG. 6. Comparison of the mass concentration $\sigma_{jk}^{PM_{10}}(t)$ of the tracer fluid (a)–(d) and the associated rolling means $\overline{\sigma_{jk}^{PM_{10}}}(t)$ and $\overline{\sigma_{jk}^{PM_3}}(t)$ (e)–(h) for the cases ($k = 1, 2, 3, 4$) at the three observation stations ($j = 1, 2, 3$).

concentrations, $\sigma_{j2}^{PM_{10}}(t)$ and $\sigma_{j3}^{PM_{10}}(t)$, respectively, for the cases of 2.5 and 3 ft barriers at stations 2 and 3 ($j = 2, 3$) with the corresponding mass concentrations, $\sigma_{1k}^{PM_{10}}(t)$ ($k = 2, 3$), at station 1 [Figs. 6(b) and 6(c)]. The observations on the inside of the barrier at station 1 dwarf those at the stations 2 and 3 on the outside of the barrier. The rolling mean mass concentrations, $\overline{\sigma_{jk}^{PM_N}}(t)$ ($j = 1, 2, 3$, $k = 2, 3$; $N = 3, 10$), are shown in Figs. 6(f) and 6(g). For case $k = 2$, the mean concentrations over the period of observation ($t = t_e$), $\overline{\sigma_{22}^{PM_{10}}}(t_e)$ and $\overline{\sigma_{22}^{PM_3}}(t_e)$, at station 2 are, respectively, 11% and 14% of the corresponding concentrations $\overline{\sigma_{12}^{PM_{10}}}(t_e)$ and $\overline{\sigma_{12}^{PM_3}}(t_e)$ at station 1. At station 3, the mean concentrations $\overline{\sigma_{32}^{PM_{10}}}(t_e)$ and $\overline{\sigma_{32}^{PM_3}}(t_e)$ are both approximately 2% of the corresponding concentrations $\overline{\sigma_{12}^{PM_{10}}}(t_e)$ and $\overline{\sigma_{12}^{PM_3}}(t_e)$ at station 1. For case $k = 3$, the mean concentrations, $\overline{\sigma_{23}^{PM_{10}}}(t_e)$ and $\overline{\sigma_{23}^{PM_3}}(t_e)$, at station 2 are, respectively, 9% and 6% of the corresponding concentrations $\overline{\sigma_{13}^{PM_{10}}}(t_e)$ and $\overline{\sigma_{13}^{PM_3}}(t_e)$ at station 1 and the mean concentrations $\overline{\sigma_{33}^{PM_{10}}}(t_e)$ and $\overline{\sigma_{33}^{PM_3}}(t_e)$ at station 3 are, respectively, 6% and 3% of the corresponding concentrations $\overline{\sigma_{13}^{PM_{10}}}(t_e)$ and $\overline{\sigma_{13}^{PM_3}}(t_e)$ at station 1.

C. Case of 3 ft barrier with an opening ($k = 4$)

Figures 3(j)–3(l) depict the sequence of captured images of the spread of the simulated cough in the presence of the 3 ft high barrier with a 5 × 12 in opening at the bottom. The images again show how the turbulent aerosolized droplet-laden air jet spreads in a boundary layer along the surface of the barrier in the form of an expanding turbulent vortex ring [Figs. 3(j) and 3(k)] once the jet impinges onto the barrier. However, significant portions of the droplets are observed [Figs. 3(k) and 3(l)] to spread to the outside via the bottom opening in the barrier while a portion again spreads over and around the barrier [Fig. 3(l)].

The leakage of the aerosols on the outside is captured in Fig. 3(m), taken from the other side of the barrier through repositioning of the laser source and the camera.

Corresponding particle counts at the three observation stations are shown in Figs. 4(j)–4(l). The significant passage of the aerosols from the opening at the bottom of the barrier to the outside of the barrier is reflected in the peaks observed in particle count measurements at stations 2 and 3 for this case [Figs. 4(k) and 4(l)]. The total particle count over the period of observation for mean droplet diameter size $\leq 1\ \mu$m at station 2 exceeded that at station 1 [Fig. 5(d)], suggesting possible occurrence of coalescence of smaller droplets in the more confined inside region, coupled with extended suspension of the smallest droplets in air. The counts at station 2 across the particle sizes in this case were higher than in the cases of the two barriers without any openings ($k = 2, 3$). The associated significant leakage of mass concentration to the outside of the barrier can be seen in Fig. 6(d), and the concentration at station 2 just outside of the barrier peaking 10–15 s following the peak at station 1. The rolling mean mass concentrations, $\overline{\sigma_{j4}^{PM_N}}(t)$ and $\overline{\sigma_{j4}^{PM_N}}(t)$ ($j = 1, 2, 3$; $N = 3.\ 10$), are shown in Fig. 6(h). The mean concentrations over the period of observation ($t = t_e$), $\overline{\sigma_{24}^{PM_{10}}}(t_e)$ and $\overline{\sigma_{24}^{PM_3}}(t_e)$, at station 2 are, respectively, 42% and 46% of the corresponding concentrations $\overline{\sigma_{14}^{PM_{10}}}(t_e)$ and $\overline{\sigma_{14}^{PM_3}}(t_e)$ at station 1 (Table I), the levels being significantly higher than in the cases of barrier without an opening ($k = 2$ and 3). At station 3, the mean concentrations $\overline{\sigma_{34}^{PM_{10}}}(t_e)$ and $\overline{\sigma_{34}^{PM_3}}(t_e)$ are, respectively, 9% and 7% of the corresponding concentrations $\overline{\sigma_{14}^{PM_{10}}}(t_e)$ and $\overline{\sigma_{14}^{PM_3}}(t_e)$ at station 1.

D. Case of 3 ft barrier with an opening and ambient back airflow ($k = 4^*$)

The above-mentioned observations were made in a laboratory setting with the same background conditions, in the absence of any observable ambient airflow. Presence of airflows, such as from an air-conditioning system in a room, can significantly alter the dispersion of the droplets around the barriers. To illustrate this, tests for the case of the 3 ft barrier with an opening ($k = 4$) were repeated in the presence of an airflow from the air-conditioning system in the room that resulted in ambient air flowing from the outside to the inside through the opening in the barrier, contrary to the direction of the spreading cough jet. The speed of the ambient counter flow is estimated from video imagery to be approximately 7 cm/s. The results for this case are shown in Fig. 7. As before, when the cough jet impinges onto the

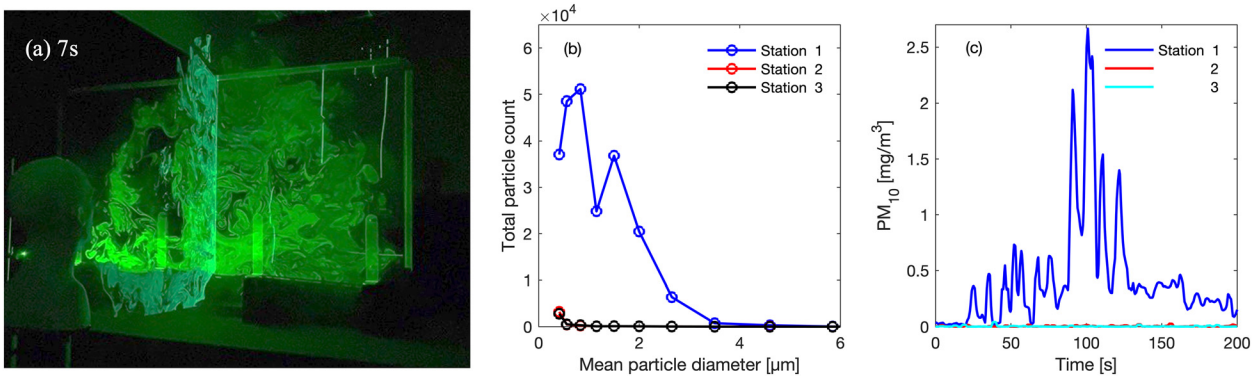

FIG. 7. Characteristics of the dispersion of the aerosols in the case of the barrier with an opening in the presence of counter ambient airflow through the opening. (a) Flow visualization at 7 s following a cough, (b) total particle count distribution, and (c) distribution of mass concentration $\overline{\sigma_{j4^*}^{PM_{10}}}(t)$ at the three observation stations ($j = 1, 2, 3$) over the observation time. Multimedia view: https://doi.org/10.1063/5.0129635.6

barrier, it spreads in a boundary layer across the barrier, and the boundary layer away from the stagnation region of the impingement thickens as it spreads as a wall jet across the barrier. However, in contrast to Figs. 3(k) and 3(m), which show the aerosols spreading to the outside via the opening in the barrier and around the barrier, Fig. 7(a) (Multimedia view) for the same case in the presence of the ambient counter airflow shows the boundary layer flow being impacted by the counter airflow, with the boundary layer blowing inwards both through the opening and around the barrier. This leads to better containment of the aerosols on the inside of the barrier. As a result, the corresponding distributions of total particle count and mass concentrations, $\overline{\sigma_{j4^*}^{\mathrm{PM}_{10}}}(t)$, are elevated at station 1 ($j = 1$) and remain at ambient levels at stations 2 and 3 ($j = 2, 3$) [Figs. 7(b) and 7(c)]. The corresponding blocking efficiencies [Eq. (2)] are over 99%.

E. Comparisons between cases

In order to provide a comparison between the cases, we follow[16] and consider efficiencies of the barriers in blocking PM_{10} and PM_3 aerosols as given by

$$\eta_{jk}^{\mathrm{PM}_{10}} = 1 - \frac{r_{jk}^{\mathrm{PM}_{10}}}{r_{j1}^{\mathrm{PM}_{10}}}, \quad \eta_{jk}^{\mathrm{PM}_3} = 1 - \frac{r_{jk}^{\mathrm{PM}_3}}{r_{j1}^{\mathrm{PM}_3}}, \tag{2}$$

where $r_{jk}^{\mathrm{PM}_N} = \overline{\sigma_{jk}^{\mathrm{PM}_N}}(t_e)/\overline{\sigma_{1k}^{\mathrm{PM}_N}}(t_e)$ is the ratio of mean mass concentrations of PM_N ($N = 10, 3$) aerosols at observation stations $j = 2, 3$ over the period of observation t_e for the different cases ($k = 2, 3, 4$) considered. The barrier efficiencies, for the set of three tests conducted for each case, are provided in Table II.

The 2.5 and 3 ft barriers ($k = 2, 3$) without any opening or opening at the bottom effectively reduced PM_{10} and PM_3 mass concentration levels just outside the barrier (station 2) by over 90% and over 82%, respectively, over their values in the absence of the barrier ($k = 1$). The relative reductions at the downstream location (station 3) were over 88% for PM_{10} and over 78% for PM_3 aerosols. The 3 ft barrier performed marginally better than the 2.5 ft barrier in the test cases considered.

For the same background conditions without any ambient airflow, the 3 ft barrier with an opening at the bottom was less effective, reducing PM_{10} and PM_3 mass concentration levels of the aerosols just outside the barrier at station 2 by only 28–59% and 30–42% of PM_3, respectively, of their value in the absence of the barrier case of no barrier ($k = 1$). The corresponding relative reductions at the further downstream location on the outside (station 3) were over 70–88% for PM_{10} and 86% for PM_3 aerosols. Overall, the results suggest that barriers are block PM_{10} particle concentration levels or containment efficiency of the barriers was better than for PM_3 concentrations, presumably since the smaller droplets provide less resistance to the air flow than the larger size droplets, and therefore, propagate better around the barriers and, in case $k = 4$, through the opening in the barrier.

The performance of the 3 ft barrier with the opening changed dramatically in the presence of an ambient back airflow (case $k = 4^*$), resulting in reductions of 99% of both PM_{10} and PM_3 mass concentration levels at both stations 2 and 3 outside the barrier over their values in the absence of the barrier ($k = 1$).

IV. DISCUSSION

Overall, our observations illustrate the benefit of a barrier in mitigating the spread of airborne aerosol-sized droplets from a cough across a room in a typical workplace setting. The observations suggest that a placement of a 3 or 2.5 ft high by 3 ft wide plexiglass barrier with no openings in the barrier 20 in from the source of a cough would be effective in reducing the PM_{10} and PM_3 mass concentration levels of droplets emitted in the cough by over 90% and 82%, respectively, at 2.2 ft from the source of the cough, and by over 88% and 78% at 4.75 ft from the source, in comparison with the case in the absence of the barrier. This is taking account of the spread of the aerosols around the barrier and considering cough jet source to be centered with respect to the barrier. The observations were made in the laboratory in the absence of any measurable ambient airflow in the room.

Under the same background conditions, the observation suggest that inclusion of a 12 × 5 in opening at the bottom of the 3 ft barrier results in significant deterioration of the effectiveness of the barrier, with reductions of only 28–59% of PM_{10} and 30–42% of PM_3 droplet mass concentrations at 2.2 ft from the cough source and 70–88% and 86% at 4.75 ft from it, in comparison with the case in the absence of the barrier. The results contrast with those of Ref. 16 who in their laboratory study reported around 70% reduction in PM_3 aerosol counts for similar sized barriers each with an opening at the bottom. The differences may be associated with likely differences in the laboratory conditions as well as the fact that the cough simulator in their study was located 30 in from the barrier, instead of 20 in as in the present study. Impact of variability in the laboratory conditions is clearly demonstrated by the case considered here (case $k = 4^*$), where an ambient back airflow dramatically resulted in the effectiveness of the 3 ft barrier with an opening at the bottom increasing from 28–59% to over 99%. Application of a plexiglass barrier in a room, therefore, requires careful consideration of the ventilation in the room as well as the type and size of the barrier and the impact of the placement of one or more barriers in a room on the room ventilation. Other factors that need to be

TABLE II. Aerosol blocking efficiencies of barriers.

	Blocking efficiency		Blocking efficiency	
	Station 2, $\eta_{2k}^{\mathrm{PM}_{10}}$ (%)	Station 3, $\eta_{3k}^{\mathrm{PM}_{10}}$ (%)	Station 2, $\eta_{2k}^{\mathrm{PM}_3}$ (%)	Station 3, $\eta_{3k}^{\mathrm{PM}_3}$ (%)
2.5 or 3 ft barrier ($k = 2, 3$)	90–99	88–99	82–97	78–98
3 ft barrier with an opening ($k = 4$)	28–59	70–88	30–42	86
3 ft barrier with an opening and ambient back airflow ($k = 4^*$)	>99	>99	>99	>99

considered include the dispersion of the aerosols contained by a barrier on the inside region of the barrier and its potential impact on susceptible individuals who may be present behind the source of the cough.

ACKNOWLEDGMENTS

The work was supported by the Centers for Disease Control and Prevention, USA, under Broad Agency Announcement (BAA) (No. 75D30121C10566). The authors have benefited from discussions with Lee Portnoff at NPPTL/NIOSH/CDC.

AUTHOR DECLARATIONS

Conflict of Interest

The authors have no conflicts to disclose.

Author Contributions

Manhar R. Dhanak: Conceptualization (lead); Data curation (equal); Formal analysis (lead); Funding acquisition (lead); Investigation (lead); Methodology (lead); Project administration (lead); Supervision (equal); Visualization (lead); Writing – original draft (lead); Writing – review & editing (equal). **Adriana Mckinney:** Data curation (lead); Investigation (equal); Visualization (equal). **Siddhartha Verma:** Conceptualization (equal); Investigation (equal); Writing – review & editing (equal). **John Frankenfield:** Conceptualization (supporting); Data curation (equal); Investigation (equal); Methodology (equal); Visualization (equal).

DATA AVAILABILITY

The data that support the findings of this study are available from the corresponding author upon request.

REFERENCES

[1]T. P. Weber and N. I. Stilianakis, "Inactivation of influenza A viruses in the environment and modes of transmission: A critical review," J. Infect. **57**(5), 361–373 (2008).
[2]R. Tellier, "Review of aerosol transmission of influenza A virus," Emerging Infect. Dis. **12**, 1657–1662 (2006).
[3]W. F. Wells, "On air-borne infection: Study II—droplets and droplet nuclei," Am. J. Epidemiol. **20**, 611–618 (1934).
[4]J. P. Duguid, "The size and the duration of air-carriage of respiratory droplets and droplet-nuclei," J. Hyg. **44**, 471–479 (1946).
[5]Y. Li, G. M. Leung, J. W. Tang *et al.*, "Role of ventilation in airborne transmission of infectious agents in the built environment—A multidisciplinary systematic review," Indoor Air **17**, 2–18 (2007).
[6]M. Bagherirad, P. Trevan, M. Globan, E. Tay, N. Stephens, and E. Athan, "Transmission of tuberculosis infection in a commercial office," Med. J. Australia **200**, 177–179 (2014).
[7]J. Ye, Z. Ai, and C. Zhang, "A new possible route of airborne transmission caused by the use of a physical partition," J. Build. Eng. **44**, 103420 (2021).
[8]P. Epple, M. Steppert, M. Florschütz, and P. Dahlem, "Partition walls as effective protection from bio-aerosols in classrooms—An experimental investigation," GMS Hyg. Infect. Control. **16**, 1–10 (2021).
[9]A. Foster and M. Kinzel, "SARS-CoV-2 transmission in classroom settings: Effects of mitigation, age, and Delta variant," Phys. Fluids **33**, 113311 (2021).
[10]W.-H. Ching, M. K. H. Leung, D. Y. C. Leung, Y. Li, and P. L. Yuen, "Reducing risk of airborne transmitted infection in hospitals by use of hospital curtains," Indoor Built Environ. **17**(3), 252–259 (2008).
[11]Z. Liu, R. Li, Y. Wu, R. Ju, and N. Gao, "Numerical study on the effect of diner divider on the airborne transmission of diseases in canteens," Energy Build. **248**, 111171 (2021).
[12]M. Abuhegazy, K. Talaat, O. Anderoglu, and S. V. Poroseva, "Numerical investigation of aerosol transport in a classroom with relevance to COVID-19," Phys Fluids **32**(10), 103311 (2020).
[13]M. Mirzaie, E. Lakzian, A. Khan, M. E. Warkiani, O. Mahian, and G. Ahmadi, "COVID-19 spread in a classroom equipped with partition—A CFD approach," J. Hazard Mater. **420**, 126587 (2021).
[14]C. Ren, C. Xi, J. Wang, Z. Feng, F. Nasiri, S.-J. Cao *et al.*, "Mitigating COVID-19 infection disease transmission in indoor environment using physical barriers," Sustainable Cities Soc. **74**, 103175 (2021).
[15]J. Lessler, M. K. Grabowski, K. H. Grantz, E. Badillo-Goicoechea, C. J. E. Metcalf, C. Lupton-Smith, A. S. Azman, E. A. Stuart, and T. Household, "COVID-19 risk and in-person schooling," J. Sci. **372**, 1092–1097 (2021).
[16]J. Bartels, C. F. Estill, I.-C. Chen, and D. Neu, "Laboratory study of physical barrier efficiency for worker protection against SARS-CoV-2 while standing or sitting," Aerosol Sci. Technol. **56**, 295 (2022).
[17]US Centers for Disease Control and Prevention, *Interim Infection Prevention and Control Recommendations for Healthcare Personnel During the Coronavirus Disease 2019 (COVID-19) Pandemic* (US Centers for Disease Control and Prevention, 2022).
[18]National Institutes of Health, *Proper Use of Barriers (Plexiglass/Lexan) in the Workplace* (U.S. Department of Health and Human Services, Bethesda, MD, 2022).
[19]Environmental Modelling Group, *Role of Screens and Barriers in Mitigating COVID-19 Transmission* (UK Government, London, UK, 2021).
[20]S. Verma, M. Dhanak, and J. Frankenfield, "Visualizing the effectiveness of face masks in obstructing respiratory jets," Phys. Fluids **32**, 061708 (2020).
[21]S. Verma, M. Dhanak, and J. Frankenfield, "Visualizing droplet dispersal for face shields and masks with exhalation valves," Phys. Fluids **32**, 091701 (2020).
[22]S. Sousan, S. Regmi, and Y. M. Park, "Laboratory evaluation of low-cost optical particle counters for environmental and occupational exposures," Sensors **21**, 4146 (2021).
[23]J. W. Guzlntner, John N. B. Livingood, and P. Hrycuk, "Survey of literature on flow characteristics of a single turbulent jet impinging on a flat plate," Report No. TN D-5652 (NASA, 1970).